Laser Ablated Surface Engineering: From Discovery to Machine Application

R. Valizadeh[1], O.B. Malyshev[1], T. Sian[1,2], J.S.Colligon[1], Q. Li[3], W. Perrie[3],

[1]ASTeC, STFC Daresbury Laboratory, Warrington, WA4 4AD, UK
[2]The Photon Science Institute, University of Manchester, Manchester M13 9PL, UK
[3]Laser group, University of Liverpool, L69 3BX, UK

Abstract

In the past few years we have established that Laser Ablation Surface Engineering (LASE) is a very effective way of producing surfaces which have Secondary Electron yields (SEY) < 1. These can be achieved with a variety of laser pulse durations from nano- to pico seconds. Unfortunately the features (i.e. moderately deep grooves and nano-particulates) that help to reduce the SEY also produce undesirable effects such as an increase in surface impedance and loose particulates. In this paper we have examined several techniques to minimise these unwanted effects. For reducing the depth of the surface altered layer femtosecond laser pulses are used which generate wavelength-scale surface structures with directionality and periodicity, known as laser-induced periodic surface structure (LIPSS). The reduction in SEY in most cases has been less effective, but a few laser processing parameters have produced reasonable SEY values (less than 1 for primary electron energy below 400 eV). The role of processing atmosphere has also been examined where the processing in inert gas (Ar) resulted in a non-stoichiometric oxide surface as compared with air laser treated surfaces that resulted in fully oxidised state. The latter inhibited the growth of carbon on the surface but still aged with time and yielded a higher SEY after several months of exposure to air.

INTRODUCTION

In particle accelerators such as the LHC [1-3], KEKB [4], DAΦNE [5], RHIC [6] and others, the secondary electron emission (SEE) can cause an electron cloud build-up inducing an increase in beam instability, beam losses, emittance growth, vacuum pressure increase, a reduction in the beam lifetime, or, it can lead to additional heat loads on a cryogenic vacuum chamber. It was specifically highlighted in many scientific presentation that the high luminosity upgrade for the LHC (known as HL-LHC) requires complete elimination of the electron cloud which would be only possible when the beam screen surface SEY could be reduced, ideally to less than unity.

SEE is a phenomenon that negatively affects particle accelerators. It can be described as follows: initial electrons appear from residual gas ionisation by beam particles or due to photoelectron emission (PEE) from beam pipe walls, from synchrotron radiation emitted by accelerated particles in the dipoles and quadrupoles. These primary electrons are accelerated in the electric field of the passing bunches and can acquire kinetic energies up to several hundreds of eV. In turn, upon colliding with the wall of the chamber, they can cause SEE. Electron multipacting can be triggered in the case of resonant conditions generated by the electromagnetic field of the beam train. Although the primary photon-induced emission and gas ionisation could be a significant source of electrons, the electron-wall impact, with energies in the range of 100 to 300 eV, can significantly increase the electron density by several orders of magnitude over the primary electron density.

It has been shown both theoretically and experimentally [3] that the e-cloud density build-up depends on the SEY function δ(E) and to minimize the effects of e-cloud, the δmax value should be less than a certain threshold value, but in all cases δmax<1 would be a sufficient condition [3,7]. Since the secondary electron yield is influenced by the wall material, surface chemistry, topography and electron energy, any deliberate mitigation mechanism is based on engineering the first three of these parameters. There are a few ways of reducing the SEY:

(a) Choice of material with low SEY (for example, Cu has lower SEY than Al);
(b) Modifying surface geometry (e.g. making grooves) [3,8];
(c) Coating with low SEY materials (such as TiN [9], Non-Evaporable Getters (NEG) [10] and amorphous carbon (a-C) [11]);
(d) Coating with low SEY microstructure (eg.: copper black, gold black;
(e) columnar NEG is better than dense) [12,13];
(f) Various combinations of above.

Recently, a low SEY < 0.9 for as-received metal surfaces modified by a nanosecond pulsed laser was reported for the first time by Valizadeh et.al. [14-16]. The technique involves rapid surface micro- and nano- restructuring at room temperature using a high power pulsed laser at various wavelengths for processing of aluminium, stainless steel and copper surfaces. The average laser energy fluence is at the ablation threshold of the substrates. The process of low SEY laser treated surfaces is the most promising solution as it is technically simple and cost effective. The influence of micro- and nano-structures induced by laser surface treatment in air of copper samples as function of various laser irradiation parameters such as peak power of laser, number of pulses per point (scan speed and repetition rate) and fluence, on the SEY has been discussed at length in our previous paper [17]. The effectiveness of the LASE has also been discussed in detail after test carried out on a section of the

SPS accelerator at CERN where the section was equipped with an e-cloud monitor [18].

The results in this paper are primarily focused on the effect of surface texturing created by the interference between the incident polarized laser light and the light scattered from the irradiated surface. The light is scattered due to surface impurities or defects, and the interference induces periodic energy density undulation on the surface. This generates wavelength-scale surface structures with directionality and periodicity, known as laser-induced periodic surface structure (LIPSS) [19-21]. This allows for formation of features in the nano-scale which is significantly smaller than achievable by direct ablation. Hence it may result in reducing the increase of surface impedance after laser treatment.

It also examines the effect of process atmosphere, effect of aging on SEY as well as the size of particle generated after laser ablation.

EXPERIMENTAL PROCEDURES

Production of LIPSS and periodic structure on stainless steel and copper

A standard Omicron sample holder fabricated from 314 SS and oxygen free copper was used as substrate for this study. A Ti-sapphire (Clark-MXR CPA 2010), of τ = 180 fs, repetition rate of f = 1 kHz and maximum average power of 30 W at λ = 775 nm was utilized for irradiation of the samples in an air atmosphere at room temperature. The diameter of the focused laser spot on each target between the points where the intensity has fallen to $1/e^2$ of the central value was varied between 10 µm. The laser beam had a Gaussian intensity profile ($M_2 \sim 1.1$) and was focused on to the target surfaces using a Nutfield scan head with 100 mm f theta lens system which is a specialised lens system in which the focal plane of the deflected laser beam is a flat surface. Figure 1 and Table 1 show the sample process identification and process laser parameters.

A facility for SEY and surface chemistry studies

A dedicated facility was designed, built and operated for SEY studies. The facility consists of three chambers as shown in Fig. 2 1: a load-lock chamber, the SEY measurement chamber, the surface treatment and the analysis chamber. After placing a sample into the load lock chamber, it was pumped there for at least 12 hours using a 210 l/s turbo-molecular pump (TMU 261, PFEIFFER Vacuum).

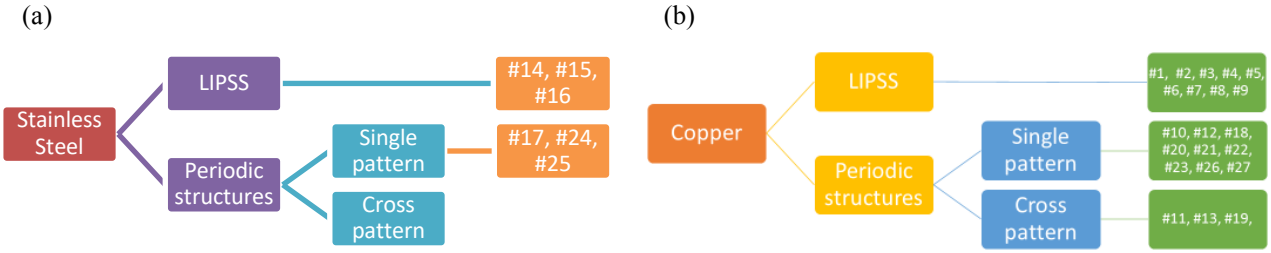

Figure 1: Sample processing identification and their maximum SEY: (a) stainless steel and (b) copper substrates.

Table 1: Laser parameters for LIPSS and periodic structure production: (a) stainless steel and (b) copper substrates.

Sample	Energy (µJ)	Hatch (µm)	Speed (mm/s)	Overscan	Ra (nm)	Width *w* (µm)	Depth *d* (µm)	*d/w*	δ_{max}
	(a) Stainless steel								
Pristine					200				
14	123	120	7.5	1	247				1.67
15	123	180	7.5	1	224				1.60
16	123	70	7.5	1	219				1.59
17	50	30	5	3	1210	13	4	0.31	1.34
24	50	30	5	5	899	14	3.5	0.25	1.51
25	50	30	5	15	1200	15	4	027	1.52
	(b) Copper								
Pristine					70				
18	20	30, 60	5	1	586	15	2.5	0.17	1.51
19	20	30, 60	5	1	666	14	3	0.21	1.56
20	50	30, 60	5	1	1120	18	4.5	0.25	1.50
21	50	30	7.5	1	483	22	2	0.09	1.65
22	20	30	10	1	179	14	0.7	0.05	1.57
23	50	30	10	1	365	20	1.5	0.08	1.60
26	75	42	5	10	9000	25	23	1.04	1.54
27	75	30	5	6	5700	18	15	0.83	1.46

The pressure of 2×10^{-9} mbar, measured using an MKS Pirani and inverted magnetron gauges, is routinely reached after overnight pumping from atmosphere. The sample is then transferred into the UHV SEY measurement chamber. The SEY measurement chamber is equipped with a combined NEG and sputter ion pump (NEXTORR® D100-5, SAES Getters), which enables a pressure of 2×10^{-10} mbar to be obtained without electron bombardment and of (2-5) $\times10^{-9}$ mbar during electron bombardment. The pressure is measured using a Leybold extractor gauge.

The schematic layout of the SEY measurements is shown in Figure 2. The electron beam with energy ranging from 80 to 1000 eV is generated by the Kimball electron gun (ELG-2/EGPS-2). The Faraday cup is made of 304L stainless steel and is a 85 mm long and 50 mm diameter cylinder with two plates on the top and bottom. The electrons enter the Faraday cup through the top 8-mm diameter hole passing through to the opposite site of the Faraday cup and bombard the sample placed in front of the 10-mm diameter hole in the Faraday cup. The beam size at the sample (full width half maximum - FWHM) has been measured with a phosphor screen and wire scanner for different electron gun parameters and electron beam energies before performing the SEY experiments. The spot size during the SEY measurements was 0.28 cm^2.

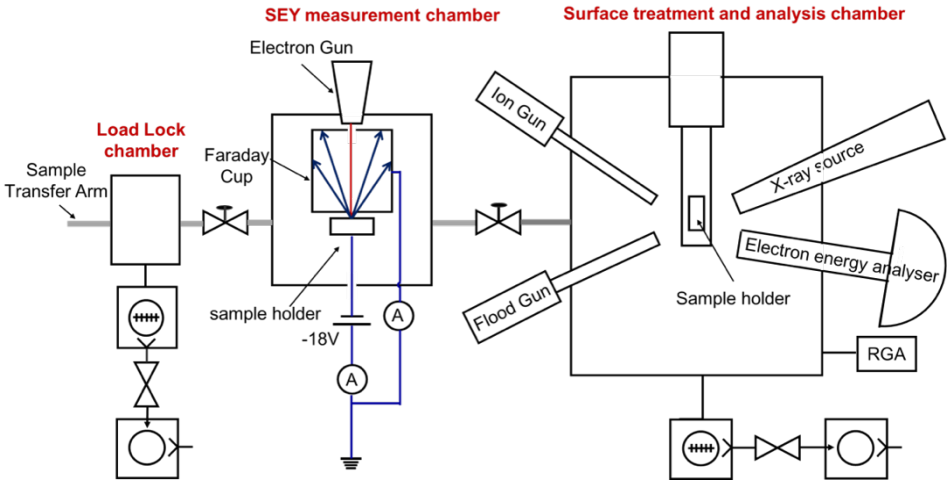

Figure 2: Schematic layout of the facility for SEY studies.

The secondary electrons are collected by the Faraday cup. The currents flowing through the sample and the Faraday cup are recorded for the SEY measurement.

The total SEY (or δ) is defined as

$$\delta = \frac{I_f}{I_\rho} = \frac{I_f}{I_s + I_f} \quad (1)$$

where I_s is the secondary electron current (including both elastic and inelastic processes) measured at the sample, I_f is the current on the Faraday cup and I_p is the primary beam current. In these experiments the net current at the sample biased at –18 V and the Faraday cup at ground potential were measured with two current amplifiers (Keithley 6517A and Keithley 6485, accuracy ±0.01%). As the SEY is very sensitive to the electron dose, the total electron dose during the SEY measurements, as a function of primary energy, was not allowed to exceed 10^{-6} C·mm^{-2}. The accuracy of the SEY measurements was estimated to be within 1% for primary electron energies between 80 and 800 eV and about 6% for primary electron energies above 800 eV.

After SEY measurements the sample can be transferred to the surface treatment and analysis chamber which is equipped with a flood gun (AG 31F, VG) used for electron conditioning (electron energy 485 eV and the accuracy of the electron dose was within 10%), an argon ion gun (PSP, ISIS 3000) with energy of 1.5 keV for surface etching and a sample heater which allows sample heating up to 300 °C. In addition the sample surface composition and chemical bonding energies can be analysed using an X-ray gun and an electron energy analyser. XPS measurements are carried out using a hemispherical analyser fitted with a five channeltron detector. Power supplies are for the spectrometer a PSP Resolve Control and, for the detectors, a PSP #705. The spectrometer was operated at 20 eV pass energy at all times and the angle between the X-ray source and electron analyser is 70 degree. Photo-electrons are excited by a non-monochromatic Al Kα X-ray source ($h\nu$ = 1463 eV) using a VG twin anode. The Al anode used at all times operated at 10 keV, 20 mA.

The surface treatment and analysis chamber is equipped with a 340 l/s turbo-molecular pump (Leybold 340M) and 1000 l/s getter pump (CapaciTorr® D-1000 Pump, SAES Getters). The base pressure of about 10^{-9} mbar was measured by a Leybold extractor gauge and the residual gas composition was monitored using a residual gas analyser (RGA, VG Thermo, VGQ).

A typical experimental procedure could involve SEY measurement of the as-received sample, followed by XPS measurement, conditioning using the diffuse-beamed

electrons from the flood gun, ion bombardment, or, thermal treatment, followed by another XPS measurement and another SEY measurement..

Particle size measurement set-up

Particle size counting measurements were carried out in an ISO 3 clean room at ETC?. Laser treated samples were exposed to nitrogen with two different pressures of 1.5 bar and 5 bar. Particle size counting measurements were performed using a particle counter situated in the clean room (Figure 3) by counting for 60 seconds for each pressure and sample. Background data was also checked before performing measurements and was found to be quite low for both the pressures of 1.5 and 5 bar.

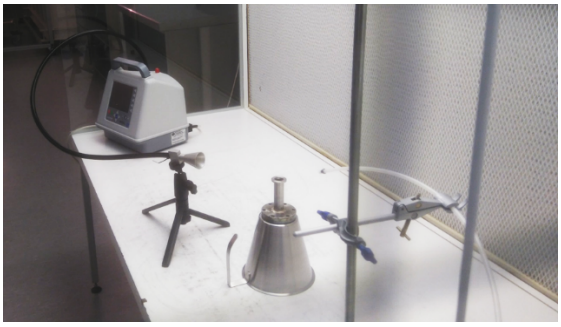

Figure 3: Particle size measurement set-up.

RESULTS AND DISCUSSION

SEY of LIPSS

Figure 4 depicts the SEY counts per second of the laser-treated SS sample with scan values higher than 1. In all cases the SEY has decreased over all the primary electron range and the δ_{max} (at E_p =300 eV), observed for the as-received untreated sample, is replaced by slowly increasing slope. The SEY rises initially for primary electron energies below 200 eV. For energies 200 eV < E_p < 400 eV the rate of increase reduces and flattens off with gradient towards the higher primary electron energy.
The decrease in SEY is not as large as the one reported previously [14-15-16] where deeper grooves (100 to 10 µm) were formed by laser ablation at higher pulse length of (τ in pico and nanosecond).

It has been shown that the reduction in SEY is due to the presence of deep grooves and the nanoparticle location on the surface [16]. For LIPSS the grooves are a factor 10 shallower and hence the reduction in SEY is not sufficiently suppressed. The value of δ_{max} for all the laser process parameters are tabulated in Table 1 for the stainless steel and copper samples.

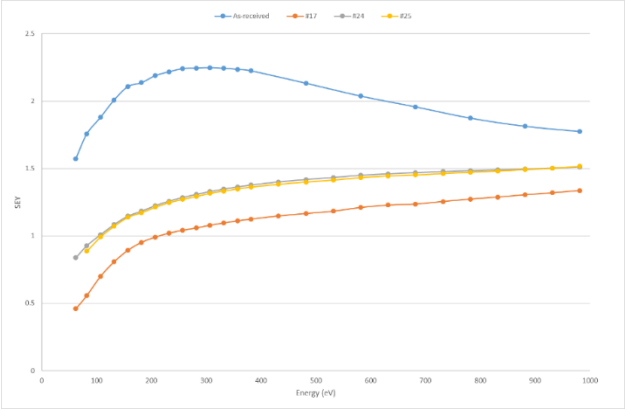

Figure 4: SEY as a function of incident electron energy for the untreated and the laser treated stainless steel samples 17, 24 and 25.

Process atmosphere

Copper substrates were laser treated in argon and air atmosphere with identical laser processing parameters. Figure 5 represents the XPS spectra of a copper substrate laser treated in an argon atmosphere for as-received and after electron bombardment for various doses at 500 eV. It can be seen that the as-received surface is in a Cu(I) oxide state and the surface is covered by a thick carbon layer. However further electron scrubbing has reduced the oxide state and promotes further carbon growth at the surface. Table 2 depicts the atomic percent of copper, oxygen and carbon at the surface for as-received and the data after each electron fluence. It can be seen that the atomic percent of copper is increasing while the oxygen atomic percent is decreasing and, at the same time, the carbon atomic percent is steadily increasing.

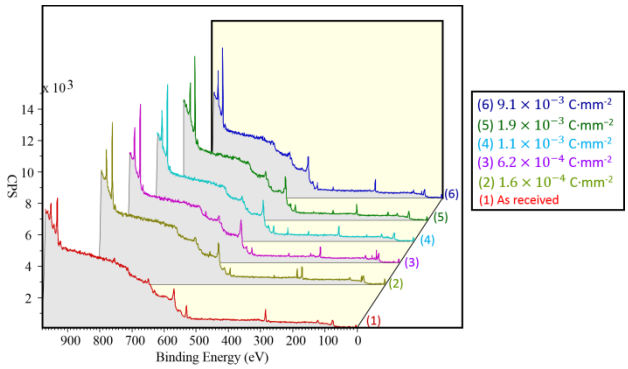

Figure 5: XPS survey spectra of as receive and electron beam scrubbing of copper sample laser treated in argon atmosphere.

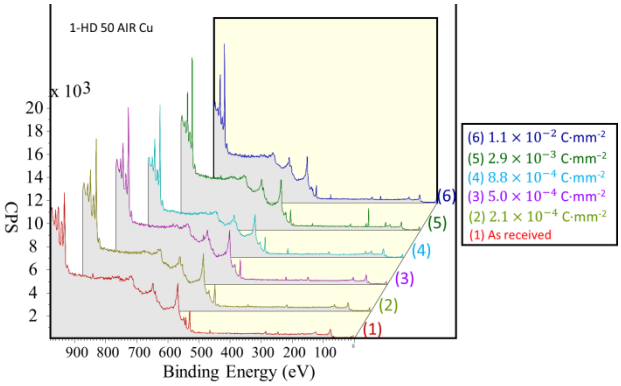

Figure 6: XPS survey spectra of as receive and electron beam scrubbing of copper sample laser treated in air atmosphere.

Figure 6 represents the XPS spectra of a copper substrate laser treated in air atmosphere for as-received and after electron bombardment for various dose at 500 eV. It can be seen that the as- received sample surface is in the Cu(II) oxide state (note the presence of satellite at biding energy of 943 eV) and the surface is covered by a thinner carbon layer.

Further electron scrubbing has lesser influence in reducing the oxide state and no further carbon growth takes place at the surface.

Table 3 depicts the atomic percent of copper, oxygen and carbon at the surface for as-received and after each experience of electron fluence. It can be seen that the overall atomic percentage of individual species (Cu, C, O) at the surface remains the same even after long electron scrubbing.

Table 2: Atomic percent of surface composition as receive and electron beam scrubbing of copper sample laser treated in argon atmosphere.

Electron dose (C/mm^2)	O1s			C1s			Cu2p		
	position	FWHM	At%	position	FWHM	At%	position	FWHM	At%
As received	531	3.11	26.6	285	2.56	63.3	932	2.49	10.1
1.6×10^{-4}	531	2.58	15.4	285	2.43	67.9	932	2.08	16.7
6.2×10^{-4}	530	2.78	22.6	285	2.43	59.6	932	2.12	17.8
1.1×10^{-3}	530	2.04	16.3	284	2.41	65.5	932	2.09	18.1
1.9×10^{-3}	530	2.16	14.7	284	2.39	69.2	932	2.07	16.1
9.1×10^{-3}	530	2.47	14.8	284	3.29	70.1	932	2.09	15.1

Table 3: Atomic percent of surface composition as receive and electron beam scrubbing of copper sample laser treated in air atmosphere.

Electron dose (C/mm^2)	O1s			C1s			Cu2p		
	position	FWHM	At%	position	FWHM	At%	position	FWHM	At%
As received	530	3.65	47.5	285	2.44	20.6	934	3.83	32.0
2.1×10^{-4}	530	2.96	58.6	285	4.58	20.0	933	2.76	21.5
5.0×10^{-4}	530	2.68	37.6	285	4.75	30.1	933	2.80	32.3
8.8×10^{-4}	530	2.71	52.1	284	2.62	22.2	932	2.09	25.7
2.9×10^{-3}	530	2.61	45.9	284	2.06	18.6	932	2.51	35.4
1.1×10^{-2}	530	2.58	44.6	284	2.81	20.0	932	2.37	35.5

Effect of sample aging on SEY

Figure 7 represents the effect of ultrasonic cleaning in acetone and data for the same sample aged for 10 months on the SEY of the copper sample laser treated with the parameters tabulated in Table 4. It can be seen that the shape of the curve stays almost the same but the SEY is shifted to a higher value for all the primary electron energies with the shift becoming larger with increasing primary electron beam energy and remaining almost constant for $E_p > 400$ eV.

Figure 8 is the SEM image of the as-received laser treated copper sample. The ten 10 to 15 µm deep grooves formed under laser treatment are completely covered with nanoparticles. The increase of SEY after the acetone cleaning is attributed to the loss of loose nanoparticles at the surface which have become separated due to ultrasonic agitation. The increase of SEY is hypothesised to be due to the build of a hydrocarbon layer while the sample was exposed to air.

Table 4: The laser processing parameters for the copper Sample 1.

Pulse duration	ps	5
Scan speed	mm/s	30
Wavelength	nm	1064
Pitch spacing	µm	5
Repetition	kHz	1.25
Power	W	5

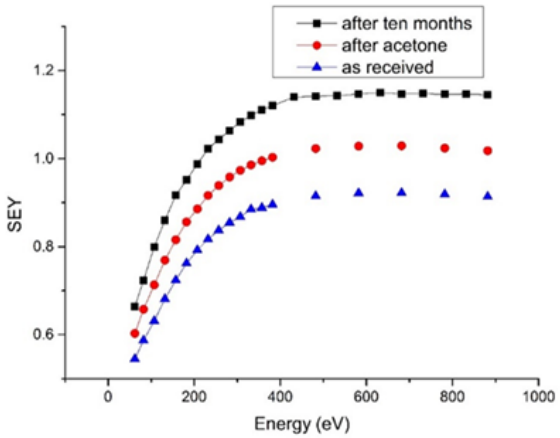

Figure 7: Effect of acetone cleaning and aging on SEY as a function of incident electron energy.

Hence extra steps should be taken to ensure the surface chemistry is not modified after laser treatment. One way of achieving such goal is to keep the surface either in vacuum or in an inert gas atmosphere.

During electron scrubbing, the process of carbon build up is done in vacuum, the carbon layer is composed of amorphous carbon which is known to have low SEY, however when the sample is exposed to air the carbon layer is composed of hydrocarbon which has high SEY.

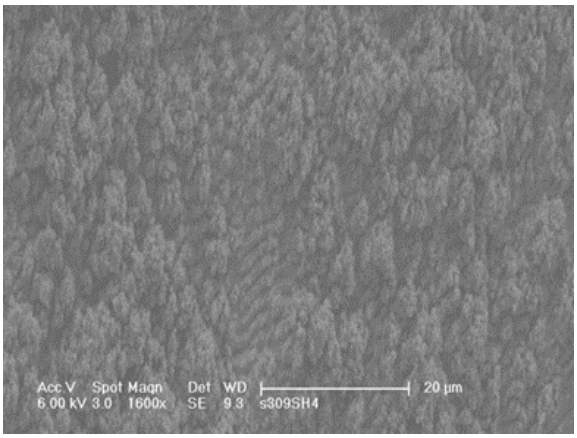

Figure 8: SEM image of as-received of a laser treated copper substrate.

Particle size determination

One of the by-products of the laser ablation is production of particulates which, if not attached strongly enough to the surface, have the potential of causing serious damage during beam delivery in particle accelerators. Hence it is vitally important to assess the size and quantity of loose particles generated after laser processing. The assessment was done using two different methods:

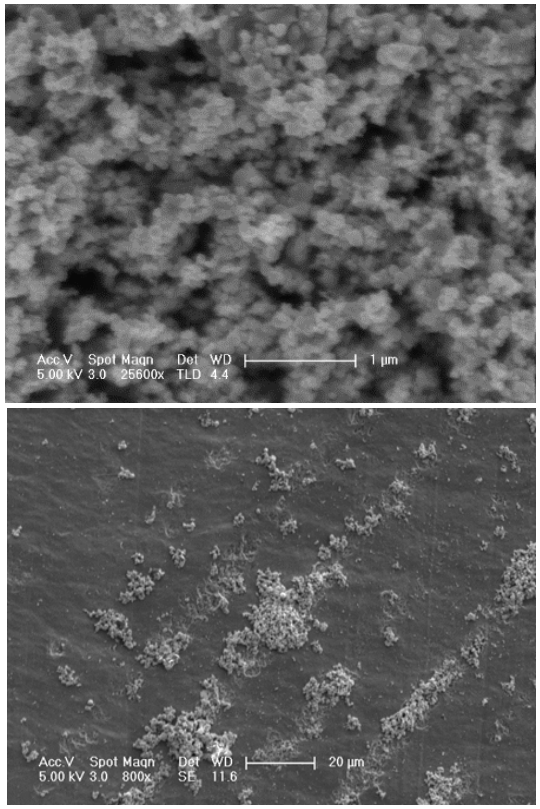

Figure 9: SEM images of laser processed copper substrate, after ultrasonic bath agitation (a), and the remaining residual at the bottom of the bicker.

(1) Ultrasonic bath agitation

Figure 9 depicts the SEM image of a copper sample, laser-irradiated with pulse length t = 5 ps and wavelength of λ = 1064 nm, scanned over with spot size of 15 µm and scan pitch of 5 µm, after ultrasonic agitation in acetone (Fig. 9a).The residual material left at the bottom of the beaker is shown in Figure. 9b. As it can be seen, although the surface has stayed to some extent intact nevertheless there is a small amount of particulates that have been detached during the agitation.

The effect of such loss of material from the surface on SEY is shown in Fig. 10 for two different scan speeds. As can be seen in both cases, the SEY has increased and more so for the higher scan speed. As mentioned above the increase can be attributed to two factors:

- Loss of particulate shown in Fig. 9b;
- Built up an hydrocarbon layer on the surface.

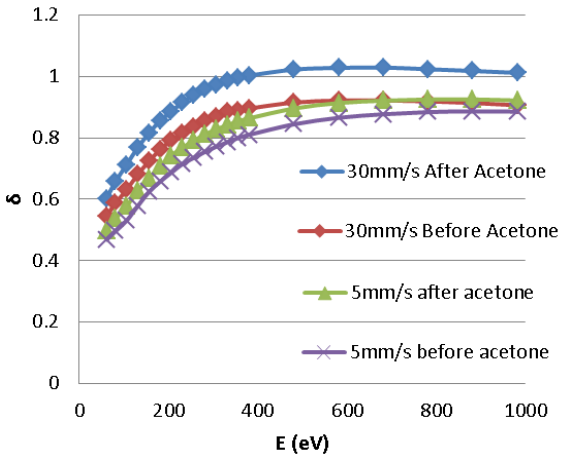

Figure 10: SEY as a function of incident electron energy for laser processed copper for as received samples and samples after ultrasonic agitation for two different scan speeds.

(2) Particle count

Figure 11 shows the the amount and the size of particles between 0.3 to 0.5 μm and 0.5 to 1 μm for samples treated in air at two different scan speeds (30 and 5 mm/s) and in an Ar atmosphere at scan speed of 5 mm/s. Polished and untreated samples were used as reference baseline samples. The detector could measure up to a particle size of 25 μm, however the largest particle observed was 1 μm in size. The largest quantity was for 5mm/s scan in air. The lowest quantity was for the sample treated in Ar which most probably is due to extra flow during laser ablation that has helped to remove any loose particles. Based on this finding it is recommended that the laser ablation should be always carried out with a flow of some kind of gas to remove the execess unwanted particulates.

CONCLUSIONS

In a previous papers we have demonstrated that reduction of SEY with laser ablation surface engineering (LASE) is very effective to produce surfaces with the lowest SEY reported up to date These are easy to achieve (as compared with other already existing techniques), is reasonably scalable since the technology already exists for other sectors and can be easily adapted. The process can be very cost-effective, especially with the availability of new more powerful and low cost lasers offered by industry.

However, several small problems still remain such as surface impedance, loose particles and effect of aging that need to be addressed. The results in this paper have gone some way in addressing these problems and offer applicable solutions either, to completely overcome or partially reduce them.

Using a femtosecond laser, where the surface engineering is more confined to the sample surface, it will be possible to reduce the increase in the RF surface resistance induced by laser ablation. A gas flow with adequate pressure will reduce the concentration of loose particles. It may also help to change the surface chemistry at the same time. By keeping the threated surface in either vacuum or inert gas atmosphere the effect of ageing can be reduced considerably.

There is a need for more study on LASE to determine the induced increased impedance both quantitatively and qualitatively.

(a)

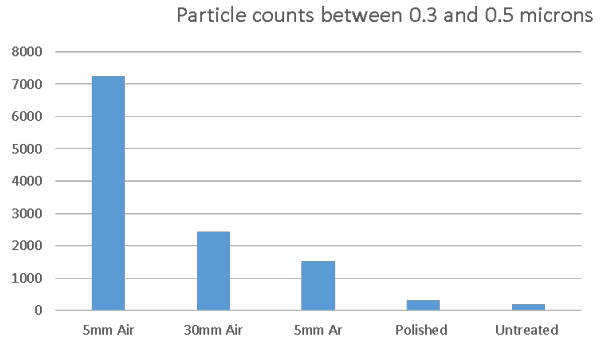

(b)

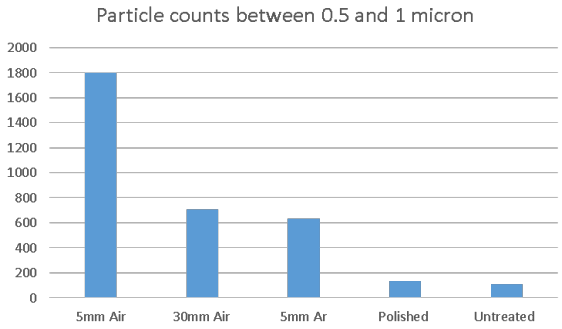

Figure 11: Particle counts for two different size range (a) 0.3 to 0.5 μm and (b) 0.5 to 1 μm.

REFERENCES

[1] G. Rumolo, G. Arduini, V. Baglin, H. Bartosik, N. Biancacci, et al. Electron cloud observations in LHC. Proc. of IPAC2011, San Sebastián, Spain (2011) p. 2862.

[2] [1] G. Rumolo, G. Arduini, V. Baglin, H. Bartosik, N. Biancacci, et al. Electron cloud observations in LHC. Proc. of IPAC2011, San Sebastián, Spain (2011) p. 2862.

[2] J. A. Crittenden, J. V. Conway, G. Dugan, M.A. Palmer, D.L. Rubin, K. Harkay, L. Boon, M.A. Furman, S. Guiducci, M.T.F. Pivi and L. Wang. Investigation into electron cloud effects in the ILC damping ring design. Proc. of IPAC-2012, New Orleans, Louisiana, USA, p. 1963 (2012).

[3] F. Zimmermann. Review of single bunch instabilities driven by an electron cloud. Phys. Rev. ST Accel. Beams 7, 124801 (2004).

[4] S. Kato, M. Nishiwaki. e-Cloud Activity of DLC and TiN Coated Chambers at KEKB Positron Ring. Proc. of Ecloud'10, Ithaca, New York, USA (2010), p. 37.

[5] D. Alesini, T. Demma, A. Drago, A. Gallo, S. Guiducci, C. Milardi, P. Raimondi, M. Zobov, S. De Santis, T. Demma, P. Raimondi. Experimental measurements of e- -2012, New Orleans, Louisiana, USA, p.1107 (2012).

[6] W. Fischer, U. Iriso. Bunch patterns and pressure rise in RHIC. Proc. of EPAC'04, Lucerne, Switzerland, July 2004, p. 914.

[7] H. Fukuma. Electron Cloud Observations and Predictions at KEKB, PEP-II and SuperB Factories. Proc. Of Ecloud'12, 5-9 Jun 2012, La Biodola, Isola d'Elba, Italy, p. 27 (2012).

[8] G. Stupakov and M. Pivi. Suppression of the effective SEY for a grooved metal surface, Proc. of ECLOUD'04, Napa, California, 19-23 April 2004, p.139 (2004).

[9.] P. He, H.C. Hseuh, M. Mapes, R. Todd and D. Weiss. Development of titanium nitride coating for SNS ring vacuum-chambers. Proc. PAC01, p.2159 (2001).

[10] W W. Fischer, M. Blaskiewicz, J. M. Brennan, H. Huang, H.-C. Hseuh, V. Ptitsyn, T. Roser, P. Thieberger, D. Trbojevic, J. Wei, S. Y. Zhang, and U. Iriso. Electron cloud observations and cures in the Relativistic Heavy Ion Collider. Phys. Rev. ST Accel. Beams 11, 041002 (2008).

[11] C. Yin Vallgren, G Arduini, J.Bauche, S. Calatroni, P. Chiggiato, K. Cornelis, P. Costa Pinto, E. Metral, G. Rumolo, E. Shaposhnikova, M. Taborelli, G. Vandoni. Amorphus carbon coatings for mitigation of electron cloud in the CERN SPS. Proc. IPAC'10, Kyoto, Japan, paper TUPD048, p. 2033 (2010).

[12] S. Wang. PhD Thesis. Loughborough University, UK, July 2016.

[13] I. Montero, L. Aguilera, M.E. Dávila, et al. Novel types of anti-ecloud surfaces. In proc. of E-CLOUD12 workshop, ELBA, Italy, 2012, p. 153.

[14] R. Valizadeh, O.B. Malyshev, S. Wang, et al. Low secondary electron yield engineered surface for electron cloud mitigation. App. Phys. Lett. 105, 231605 (2014).

[15] R. Valizadeh, O. Malyshev. Apparatus and methods relating to reduced photoelectron yield and/or secondary electron yield. Patent publication number WO2015189645 A1. 17th Dec 2015.

[16] R. Valizadeh, O.B. Malyshev, S. Wang, T. Sian, L. Gurran, P. Goudket, M.D. Cropper, N. Sykes. Low secondary electronyield of laser treated surfaces of copper, aluminium and stainless steel. In Proc. of IPAC'16, 8-13 May 2016, Busan, Korea (2016), p. 1089.

[17] R. Valizadeh, O.B. Malyshev, S. Wang, T. Sian, M. D. Cropper and N. Sykes. Reduction of Secondary Electron Yield for E-cloud Mitigation by Laser Ablation Surface Engineering. Appl. Surf. Sci. 404, 370–379 (2017).

[18] S. Calatroni, E. Garcia-Tabares Valdivieso, H. Neupert, V. Nistor A. Perez Fontenla, et al. First accelerator test of vacuum components with laser-engineered surfaces for electron-cloud mitigation. Phys. Rev. Accel. Beams 20, 113201 (2017).

[19] M. Birnbaum, Semiconductor surface damage produced by ruby lasers, J. Appl. Phys. 36 (1965) 3688.

[20] J. E. Sipe, J. F. Young, J. S. Preston, H. M. van Driel, Laser-induced periodic surface structure. I. theory, Phys. Rev. B 27 (1983) 1141–1154.

[21] S. A. Akhmanov, V. I. Emel'yanov, N. I. Koroteev, V. N. Seminogov, Interaction of powerful laser radiation with the surfaces of semiconductors and metals: nonlinear optical effects and nonlinear optical diagnostics, Sov. Phys. Uspekhi 28 (1985) 1084–1124.